Journal of Applied Polymer Science

Electrokinetic and Antibacterial Properties of Needle Like-TiO_2/Polyrhodanine Core/Shell Hybrid Nanostructures

Seyma Ozkan, H. Ibrahim Unal,[1] Ebru Yılmaz,[2] Zekiye Suludere[3]

[1]Gazi University, Science Faculty, Chemistry Department, Smart Materials Research Lab., C.P. 06500, Ankara, Turkey
[2]Gazi University, Vocational School of Health Services, C. P. 06500, Ankara, Turkey
[3]Gazi University, Science Faculty, Biology Department, C. P. 06500, Ankara, Turkey
Correspondence to: H. I. Unal (E-mail: hiunal@gazi.edu.tr)

ABSTRACT: The aim of this study was to fabricate needle like-TiO_2/polyrhodanine nanostructures by polymerizing rhodanine monomer on the TiO_2 nanoparticles' surfaces and investigate their antibacterial activities. The structural, thermal, morphological, surface and electrical properties of non-covalently functionalized nanoparticles were characterized by using FTIR, XPS, elemental analysis, TGA, XRD, SEM-EDX, TEM, contact angle, and conductivity measurements. Characterization results confirmed the formation of needle like-TiO_2/polyrhodanine (PRh) core/shell hybrid nanostructures. Alterations on the surface and electrokinetic properties of the materials were characterized by zeta (ζ)-potential measurements with the presence of various salts and surfactants. The ζ-potential of needle like-TiO_2 was observed to increase from -7.6 mV to $+28.4$ mV after forming a core/shell needle like-TiO_2/PRh nanocomposite structure and with the presence of cetyltrimethyl ammonium bromide (CTAB) surfactant. Thereby colloidally more stable dispersions were formed. Antibacterial properties of needle like-TiO_2/PRh were also tested against *Staphylococcus aureus, Klebsiella pneumoniae,* and *Escherichia coli* by various methods and they showed good antibacterial activity. The highest killing efficiency was determined for needle like-TiO_2/PRh against *E. coli* by colony-counting method as 0.95. TEM experiments also showed the immobilizations of the nanoparticles on *E. coli* and revealed the interactions between *E. coli* and the nanoparticles. © 2014 Wiley Periodicals, Inc. J. Appl. Polym. Sci. **2015**, *132*, 41554.

KEYWORDS: colloids; composites; conducting polymers; nanostructured polymers

Received 30 June 2014; accepted 24 September 2014
DOI: 10.1002/app.41554

INTRODUCTION

Polymer nanocomposites are functionally advanced materials made up of various nanoparticles, especially inorganic, either dispersed in a polymer matrix, coated by a polymer to form a core/shell structure or to compose a covalently bonded functional nanostructure. In recent years, polymer nanocomposites have been attracted much attention and have become an important material for nanotechnology. The main reasons behind this interest are design, flexibility, lower life cycle costs and continuously increasing research and industrial application areas on polymer hybrid nanocomposites due to their higher performances.[1]

Rhodanine derivatives have unique biological properties such as antibacterial, antidiabetic, antiviral and antimicrobial and thus find wide application areas.[2] Rhodanine is a Lewis base and its derivatives are good candidates to functionalize metal based nanostructures and to synthesize conducting polymers.[3] To bring about desired properties and enhance their colloidal stabilities of inorganic core/polymer shell nanoparticles, their high surface areas might be functionalized by conducting polymer chains either by covering the nanoparticles' surfaces or covalently bonding the monomers onto nanoparticles surfaces.[4] In addition, rhodanine derivatives have been reported as antimicrobial agent against *Staphylococcus aureus* (*S. aureus*) strains and other some bacteria reported in the literature.[5,6] In this study, it was expected to enhance these antibacterial properties of rhodanine by composing it with needle like-TiO_2 to form core/shell hybrid nanostructures.

TiO_2 is one of the most widely investigated metal oxide, because of its photo catalytic, light scattering, biocompatible, self-cleaning and antimicrobial properties which enables it to be used in different fields.[7] In recent years, TiO_2 is preferred for the production of materials having specific and desired properties due to its crystalline structure and different morphologies, i.e., nanorod,[8] needle-like,[9] nanosheet,[10] cubic,[11] and spherical[12] which are readily available or to be synthesized.[13]

© 2014 Wiley Periodicals, Inc.

In colloidal systems, electrical properties of particles' surfaces can be characterized by electrokinetics method measuring zeta(ζ)-potentials of dispersed particles. ζ-potential is a surface charge of a particle in a specific medium which provides information on the colloidal stability of a colloidal system by determining the thickness of electrical double layer around a suspended particle. ζ-potential measurements enable us to understand, to control and/or to determine electrical double layer or surface potential of a dispersed system. It is also an important tool to observe, control or establish dispersed (requires high ζ-potentials) or aggregated (requires low ζ-potentials) process parameters.[14]

Infections by pathogenic microorganisms are of great concern in many areas of daily life. Generally, these infections are combated with antimicrobial agents, which are susceptible to their actions. Particularly problematic ones are the resistant microorganisms that mutate their genes rapidly and easily, which make their eliminations impossible or difficult.[15] For instance, *S. aureus* is a Gram positive bacterium which commonly colonizes on human skin and mucosa without causing severe problems and also one of the major causes of hospital originated infections.[16] *Klebsiella pneumoniae (K. pneumoniae)* is a virulent Gram negative organism that causes urinary tract infections and pneumonias.[17] *Escherichia coli (E. coli)* is a Gram negative bacterium which normally lives in the intestines of people and animals and can cause urinary tract infections and diarrhea.[18] It is well known that, nanoparticles having larger surface area to aspect ratio provide excellent contact with bacterial cell walls and results in good antibacterial properties. As classified by Tenover, antibacterial agents are categorized according to their principal mechanism of actions, which are frequently discussed in the literature and are often categorized according to their four mechanism of action (i) the interactions with cell walls of bacteria, (ii) inhibition of bacteria from protein synthesis, (iii) interference of bacteria during the nucleic acid synthesis, (iv) inhibition of a metabolic pathway, and disorder of membrane structure of bacteria.[19–23]

Polymeric materials, acting as matrix, having antimicrobial properties acquired much attention from both academia and industry. To use for antibacterial purposes, hydrophilicity, molecular weight, and long-term activity of polymeric materials have to be taken in to account since they play a great role on the final antimicrobial properties of the materials. That is why fabrication of novel polymers or polymer nanocomposites, having antibacterial activities, are of great interest to scientists working in this field.[22]

Herein, we report the fabrication of novel non-covalently functionalized needle like-TiO_2/polyrhodanine (PRh) core/shell conducting nanocomposites by a simple chemical procedure, with lower cost, no sophisticated instruments for preparations, without disrupting the intrinsic structure and electronic network of rutile TiO_2. Their full characterizations with various techniques and electrokinetic properties are discussed below. Positive and enhanced antibacterial efficacies of needle like-TiO_2/PRh core/shell conducting nanocomposite were investigated against *S. aureus, K. pneumoniae* and *E. coli* by colony-counting methods, after determining the interactions between the nanoparticles and *E. coli* by TEM method. The results have indicated that this nanocomposite could be a good candidate material for future long-term antibacterial applications.

EXPERIMENTAL

Materials

All the chemicals were provided from Sigma (Germany) and used as received. Needle like-TiO_2 was obtained from Nanostructured and Amorphous Materials (USA) and used as received.

Characterizations of the Materials

ATR-FTIR Spectroscopy. For structural characterizations, ATR-FTIR spectroscopy measurements of the samples were carried out using Brucker Vertex80 instrument (UK).

XPS Spectroscopy. Chemical characterizations of the samples were determined using SPECS ESCA Model XPS instrument with MgKα radiation ($\lambda = 0.15406$ nm) under 7.6×10^{-7}atm vacuum (METU Central lab.) After peak fitting of the C1s spectrum all the spectra were recorded on the aliphatic C1s component at the binding energy of 285.0 eV.

Elemental Analysis. Elemental analyses of the samples were carried out by Thermo-Scientific Flash 2000 model (USA) CHNS Elemental Analyzer.

TGA Analysis. Thermogravimetric analysis of the samples were carried out using TA Instruments TGA Q-500 model (USA) Thermogravimetric Analyzer under nitrogen atmosphere between 30 and 700°C at a heating rate of 10° min^{-1} and also under $O_{2(g)}$ atmosphere between 700 and 900°C at the same heating rate.

XRD Measurements. For morphological characterizations, X-ray diffraction analyses (XRD) of the samples were carried out as powders using GNR APD 2000 PRO Model XRD instrument with a CuK_α radiation ($\lambda = 0.15406$ nm at 40 mV and 40 mA).

Electron Microscopy Measurements. Scanning electron microscopy (SEM) studies of the samples were carried out using Jeol JSM 6060 LV Model instrument (USA) after coating with gold in a sputter coater. Transmission Electron Microscopy (TEM) measurements were carried out using JEOL JEM-1400 Model TEM instrument. The samples were dispersed in ethanol and subjected to ultrasonication for 10 min. Then the samples were placed onto a carbon grid and dried. In addition to these treatments, needle like-TiO_2/PRh nanocomposites were also subjected to uranyl staining.

Surface Characterization. For surface characterization, contact angle measurements were carried out using KSV CAM 200 Model Instrument (USA) (Selcuk University, Dept. of Chemistry). During the measurements, volumes of the drops were kept at 3 μL and the averages of at least five data were recorded as contact angle values which were calculated by the software of the device (Olympus Micro DP70 Ver. 01.02).

Conductivity Measurements. The conductivities of the samples were determined by four-probe technique by using FPP-460A model four-probe equipment (Entek Elektronik, Turkey).

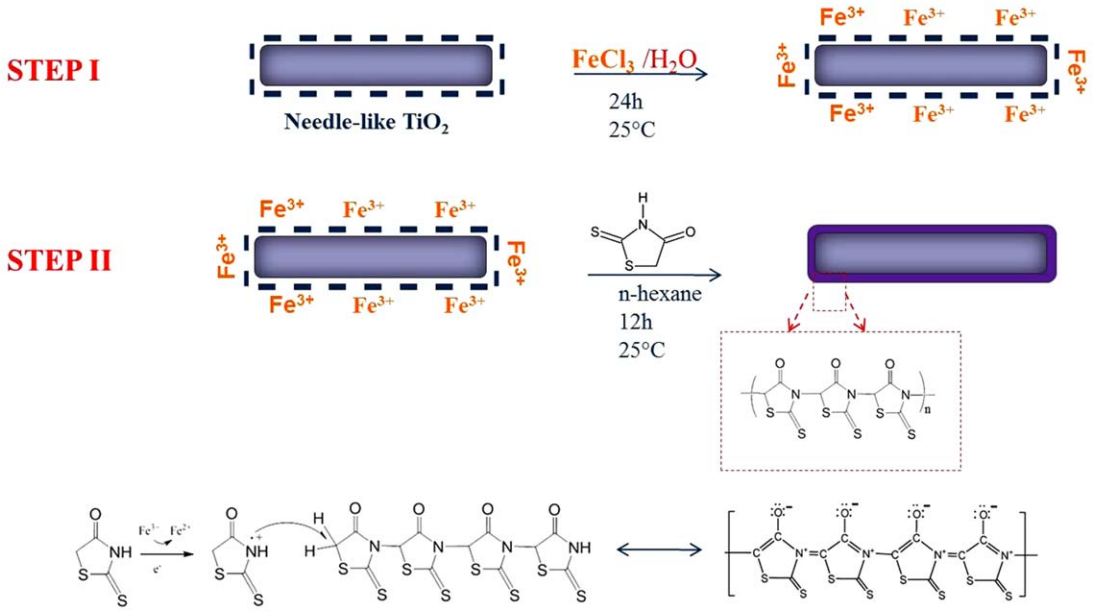

Figure 1. Schematic illustration of the fabrication of needle like-TiO_2/PRh core/shell nanoparticles. [Color figure can be viewed in the online issue, which is available at wileyonlinelibrary.com.]

Synthesis of Needle Like-TiO_2/Poly(rhodanine) Core/Shell Nanocomposite

To prepare Fe-ion coated TiO_2 nanoparticles, needle like-TiO_2 nanoparticles and $FeCl_3$ were dispersed in 100 mL deionized water by taking the weight ratio of TiO_2 : $FeCl_3$ as 1 : 1 and vigorously stirred at room temperature for 24 h. After centrifugation, Fe^{3+}ion-impregnated TiO_2 particles were obtained and dried in a vacuum oven at 25°C. Then, 0.5 g of Fe^{3+} ion-treated TiO_2 nanoparticles were dispersed in 100 mL of n-hexane by sonication for 30 min. Rhodanine monomer (75 μmol) was introduced drop wise into the reactor and the chemical oxidation polymerization of rhodanine proceeded on the surfaces of needle like-TiO_2 nanoparticles with vigorous stirring at 25°C for 24 h. After completion of the reaction, needle-like TiO_2/PRh core/shell nanoparticles were obtained by centrifugal precipitation, washed with excess deionized water to remove any residual reagents present and dried in a vacuum oven at 100°C for 24 h. The reaction procedure is schematically

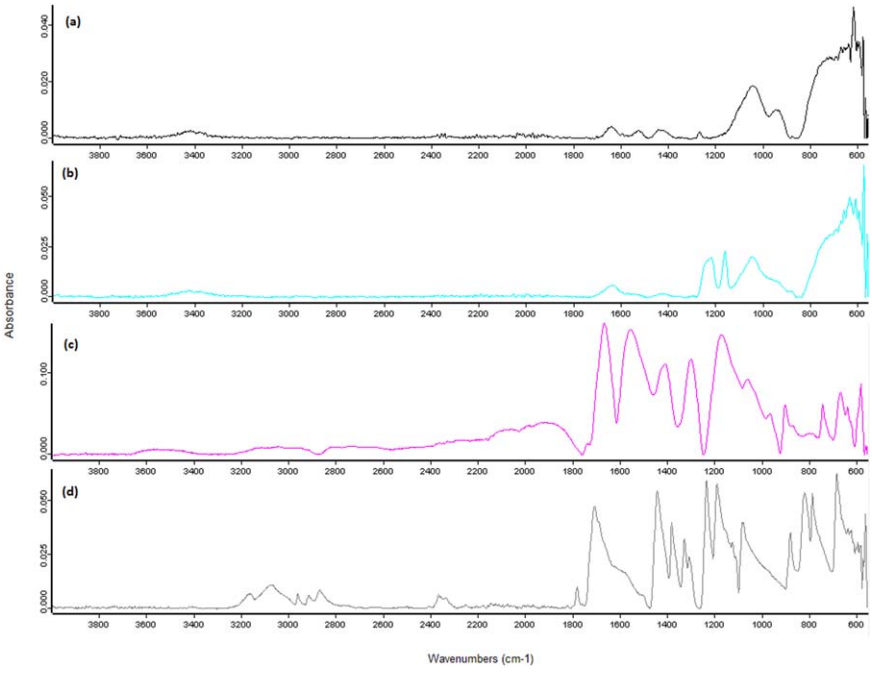

Figure 2. FTIR spectra of (a) needle like-TiO_2, (b) rhodanine, (c) PRh, (d) needle like-TiO_2/PRh. [Color figure can be viewed in the online issue, which is available at wileyonlinelibrary.com.]

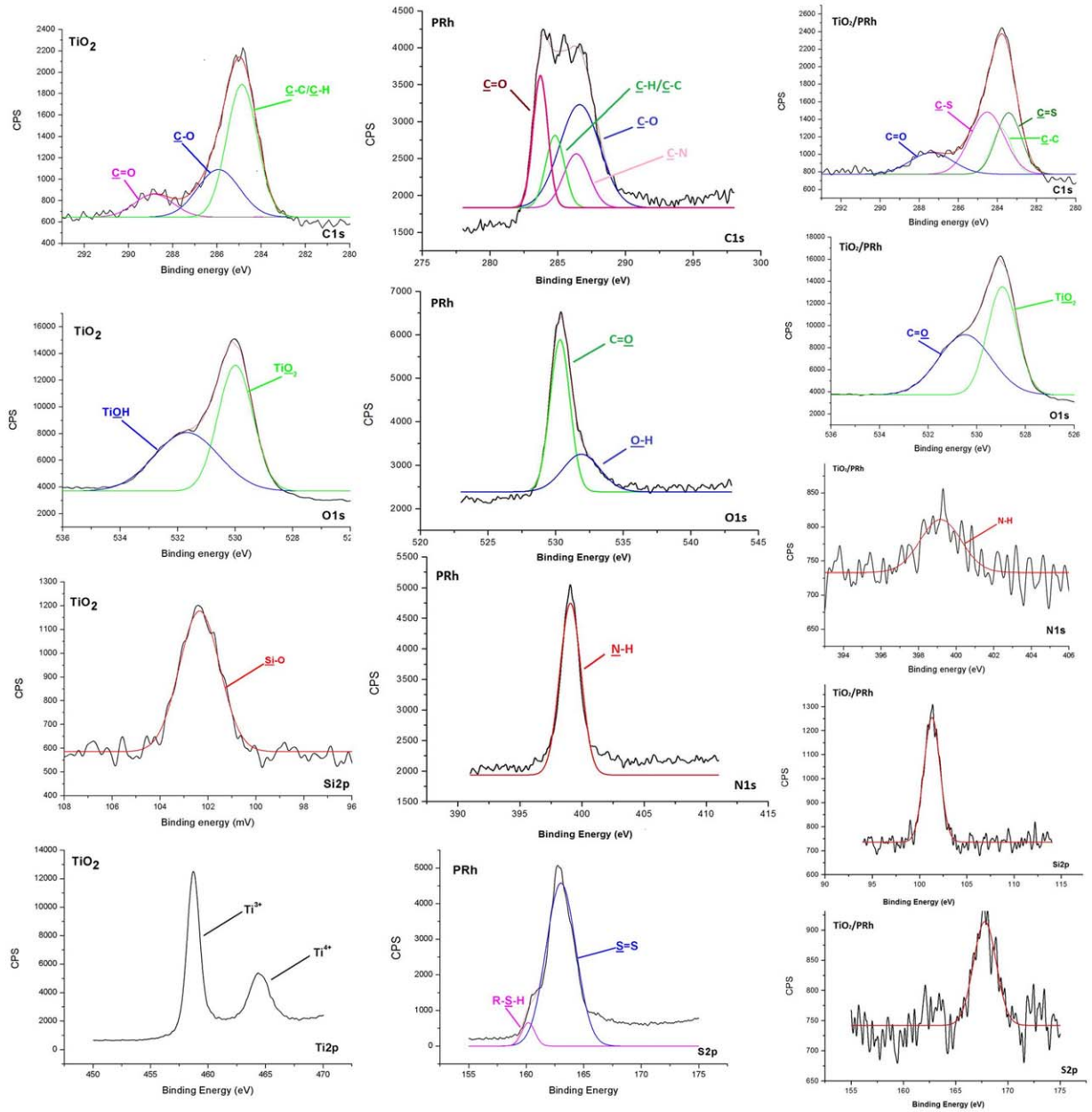

Figure 3. XPS core level spectra for (a) needle like-TiO_2, (b) PRh, (c) needle like-TiO_2/PRh. [Color figure can be viewed in the online issue, which is available at wileyonlinelibrary.com.]

shown in Figure 1. The nanocomposite particles were then subjected to various characterizations, electrokinetic measurements and antibacterial activity tests.

Electrokinetic Measurements

Zeta (ζ)-potential can be converted from measured electrophoretic mobility (U_E) using the Smoluchowski's equation:

$$\zeta = \frac{\eta U_E}{\varepsilon} \quad (1)$$

Where ε is the dielectric permittivity of the solution and η is the viscosity of the dispersed phase.

The ζ-potentials of colloidal dispersions were measured by a Malvern Nano-ZS ζ-potential analyzer which works with Laser Doppler Electrophoresis technique. The optic unit contains a 4 mW He-Ne laser ($\lambda = 633$ nm). The self-optimization routine (laser attenuation and data collection time) in the Zeta-Sizer software was used for all the measurements. In aqueous medium, the ζ-potential was calculated from the electrophoretic mobility using the Smoluchowski's model, wherein the thickness of the electrical double layer is assumed to be smaller in comparison to the dispersed particle size. The electrophoretic mobility was obtained by performing an electrophoresis experiment on each of the samples and the velocity of the dispersed particles was measured using a Laser Doppler Velocimeter. The colloidal dispersions with a concentration of 0.1 g L^{-1} were prepared for the ζ-potential measurements. Each of the dispersions

Table I. Elemental Analysis Results of PRh and Needle Like-TiO_2/PRh

Sample	C %	H %	S %
PRh	26	1.1	50.3
Needle like-TiO_2/PRh	0.72	0.9	0.72

was subjected to sonication for 30 min and hold at room temperature for further 2 h to establish equilibrium. Afterwards, the supernatant liquid was taken and used for the ζ -potential measurements and the pH was adjusted immediately by MPT-2 autotitrator unit at 25°C. In this manner, effects of time, pH, various electrolytes [(cationic: NaCl, $BaCl_2$, $AlCl_3$, anionic: Na_2SO_4], surfactants (anionic: sodium dodecylsulfate, SDS, $NaC_{12}H_{25}SO_4$, cationic: cetyltrimethyl ammonium bromide (CTAB), $C_{19}H_{42}BrN$, non-ionic: Triton X-100, $C_{14}H_{22}O(C_2H_4O)n$ (where $n = 9–10$) and temperature onto the ζ-potentials of the dispersed nanoparticles were investigated.

Preparation of Bacteria Cultures

S. aureus (Gram positive), *K. pneumoniae* (Gram negative) and *E. coli* (Gram negative) bacteria cultures were prepared by cultivating in sterilized Luria–Bertani (LB) broth and then incubated overnight at 37°C in a shaking incubator. The microorganism suspensions used for the tests contained 10^6-10^7 colony-forming units (CFU) in 1 mL.

Examination of Bacteria-Nanoparticles Interactions with TEM

The preparation of samples for TEM measurements was carried out according to Tamer et al. with some modifications.[23] Before TEM measurements firstly, needle like-TiO_2 and TiO_2/PRh nanoparticles were washed with ethyl alcohol. The liquid phase was then separated by centrifugation and discarded. The precipitate was rinsed with sterile deionized-distilled water three times. *E. coli* was suspended in this water (10^7 CFU mL^{-1}), mixed with the nanoparticles, incubated at 37°C, and shaken on an orbital shaker at 100 rpm, for 60 min. For recording TEM images, a small drop of each of the sample of nanoparticles-bacteria mixtures was deposited on the formvar-carbon coated grid, negatively stained with 2% uranyl acetate and examined by TEM at 80 KV.

Antibacterial Activity Test Methods

i. ***Well diffusion method*** was the first one to investigate the antimicrobial activities of TiO_2 and rhodanine nanoparticles. For this purpose, *S. aureus, K. pneumonia*, and *E. coli* liquid cultures were prepared in brain heart infusion broth. During the experiments, needle like-TiO_2 and rhodanine were dispersed in water at concentrations of 10 mg mL^{-1}. Approximately 1 cm^3 of a 24 h broth culture containing 10^6 CFUcm^{-3} was placed in sterile Petri dishes containing 15 cm^3 of Mueller Hinton Agar, kept at 45°C, then poured into the petri dishes and allowed to solidify. Six millimeter diameter holes were then punched carefully using a sterile cork borer and completely filled with the test solutions. The plates were incubated for 24 h at 37°C, and then the inhibition zone that expected to appear around the holes in each of the plate was measured.

ii. ***Bacterial colony-counting method*** was the second one to investigate the antibacterial activities of needle like-TiO_2 and rhodanine materials. Microorganisms were cultivated in sterilized Mueller Hinton Agar broth and then incubated overnight at 37°C in an incubator. The microorganism suspensions employed for the tests contained between 10^6-10^7 CFU. Each of needle like-TiO_2 and rhodanine materials (0.1 and 0.01 mg) were prepared in sterilized test tubes and inoculated with 1.0 mL of each microorganism suspensions (*S. aureus*, *K. pneumoniae* and *E. coli*). In the test tube, 50 μL volumes were chosen as a function of contact time (min) and cultured in Mueller Hinton agar plates. The plates were incubated for 24 h at 37°C and then analyzed for the number of bacterial colonies to determine the growth inhibition rates of TiO_2 and rhodanine using eq. (2).[2,24]

$$R(\%) = \frac{A-B}{A} \times 100 \quad (2)$$

where R is the growth inhibition rate, A is the number of bacterial colonies counted from the blank solution, and B is

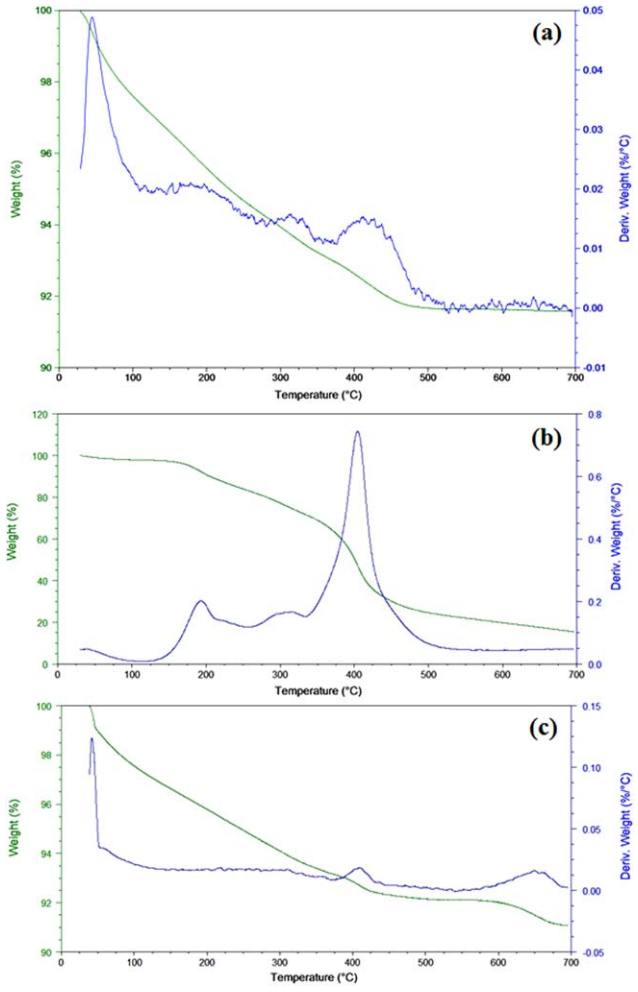

Figure 4. TGA/DTGA curves of (a) needle like-TiO_2, (b) PRh, and (c) needle like-TiO_2/PRh. [Color figure can be viewed in the online issue, which is available at wileyonlinelibrary.com.]

the number of bacterial colonies counted from the test solution. No TiO_2 and rhodanine were added to one of the test tubes, which were served as a control sample.

iii. ***Modified Kirby-Bauer disk diffusion method*** was the third one to test the antibacterial activities of TiO_2/PRh and rhodanine samples. For this purpose, disc shaped (0.6 mm × 13 mm) pellets containing 0.1 mg of needle like-TiO_2 and rhodanine were prepared by hydraulic press and tested. 100 μL of a 24 h broth culture containing 10^6 cells mL^{-1} was spread on the Mueller Hinton agar. Then, the sample pellets were placed onto the inoculated plates. The plates were then incubated for 24 h at 37°C and the inhibition zones that appeared around the holes of each disk shaped sample were measured.[16]

RESULTS AND DISCUSSION

Characterization of the Materials

ATR-FTIR Spectroscopy. ATR-FTIR spectrum of PRh (Figure 2) revealed peaks at 1662 and 1404 cm^{-1} which were corresponded to C═C and C═N^+ stretching vibrations and the peaks at 1298 cm^{-1} and 1167 cm^{-1} were corresponded to C—O stretchings, which proofed the formation of PRh when compared with rhodanine monomer.[25] For the needle like-TiO_2 particles, the peak observed at 920 cm^{-1} was due to the Ti—O—Ti stretching vibrations of TiO_2 (Figure 2). The wide peak observed at 3600–3000 cm^{-1} shows the presence of —OH groups at the surfaces of TiO_2 particles. The peak observed at 1640 cm^{-1} corresponds to the bending vibrations of adsorbed H—O—H molecules on TiO_2 particles.[26] These ATR-FTIR spectra are in accordance with the one reported in the literature by Sun et al., for room temperature synthesis of spherical mesoporous titania. For TiO_2/PRh nanocomposite, the peak observed at 3600–3000 cm^{-1} also corresponds to the bending vibrations of H—O—H molecules adsorbed on TiO_2/PRh particles (Figure 2). The peaks observed at 1637 and 1434 cm^{-1} were due to C═C and C═N^+ vibrations arising from PRh chains. Also, the peaks appeared at 1202 and 1153 cm^{-1} were due to C—O vibrations originating from rhodanine molecule.[25] These observed ATR-FTIR peaks proofed the successful synthesis of needle like-TiO_2/PRh core/shell nanocomposite and also in accordance with the data reported in the literature by Kardas for electrochemical polymerization of PRh and by Jouong et al., for silica/PRh core/shell structure.[5,25]

XPS Analyses. The above mentioned ATR-FTIR results are further confirmed by XPS analyses of the samples. Figure 3 shows the photo electron peaks of C1s, O1s, Ti2p, and Si2p for needle like-TiO_2 [Figure 3(a)], C1s, O1s, S2p for PRh [Figure 3(b)] and C1s, O1s, N1s, Si2p, and S2p for needle like-TiO_2/PRh nanocomposite [Figure 3(c)] particles. The C1s signals of the needle like-TiO_2 [Figure 3(a)] located at 285.0, 286.8, and 288.4 eV were assigned to C—C/C—H, C—O and C═O, respectively. The O1s signals of the needle like-TiO_2 located at 531.6 eV and 529.5 eV were assigned to Ti—O—Ti and Ti—OH, respectively.[27] The Ti2p signals of the needle like-TiO_2 specifically gave two large peaks located at 458.7 and 464.0 eV which are not fitted and attributed to Ti^{3+} and Ti^{4+}, respectively.[28] The Si2p signal of needle like-TiO_2 located at 102.35 eV can be assigned to Si—O binding.[29] N1s spectrum of needle like-TiO_2 was not observed. The C1s signals of PRh [Figure 3(b)] obtained from XPS measurements located at 283.8, 284.8, 286.3, and 286.6 eV can be assigned to C═O, C—H/C—C, C—N and C—O, respectively. These peaks are in accordance with the chemical bonds of rhodanine monomer and support the formation of PRh. The O1s signals of PRh located at 530.5 eV and 533.2 eV were assigned to C═O and O—H, respectively. The N1s signal of PRh displays one peak with a binding energy of 399.9 eV due to N—H band which is attributed to the presence of —NH group in the structure of PRh.[30] The S2p signal of PRh located at 160.2 and 163.0 eV can be assigned to R—S—H and S═S binding energy peaks, respectively which are in accordance with the structure of rhodanine monomer. The C1s signal of needle like-TiO_2/PRh obtained from XPS measurements [Figure3(c)] located at 284.5, 286.7, 287.4, and 289.2 eV can be assigned to C—C/C—H, C—N, C—O and C═O binding energy peaks, respectively.[31] The O1s signal of needle like-TiO_2/PRh located at 528.9 and 530.5 eV can be assigned to C═O and O—Ti binding energy peaks, respectively. The N1s signal of needle like-TiO_2/PRh displays one peak with a binding energy of 399.2 eV corresponding to the neutral amine bands, which supports the formation of PRh chains on the surfaces of needle like-TiO_2 particles. The Si2p signal of needle like-TiO_2/PRh nanocomposite located at 101.3 eV corresponds to the basic inorganic silica substrate, as expected. The S2p signal of the needle like-TiO_2/PRh displays one peak with a binding energy at 167.8 eV which corresponds to the sulfur signals. This property is a relatively high binding energy and chemical structure indicates the presence of sulfate species arising from PRh chains. The presence of N1s and S2p peaks proof the formation of needle like-TiO_2/PRh core/shell hybrid structure.

Elemental Analyses. The results obtained from elemental analysis also revealed the formation of needle like-TiO_2/PRh core/shell structure (Table I). The presence of 0.72% S element in needle like-TiO_2/PRh corresponds to 1.42% PRh which is in accordance with the approximately 2% weight loss in TGA curve within the limits of experimental error (Figure 4), and also in accordance with the data reported in the literature by Song et al., for silica/PRh core/shell nanoparticles.[5]

Thermal Behavior. The TGA and DTGA thermograms of TiO_2, PRh and needle like-TiO_2/PRh nanocomposite are given in Figure 4. The first weight loss observed for TiO_2 up to 100°C was 3 wt % and attributed to the removal of any moisture. The following 6 wt % loss was up to 500°C and attributed to the decomposition of residual organic structures present at the surfaces of TiO_2 particles.[32] PRh showed weight losses at three stages. The first weight loss of 2 wt % was occurred up to 100°C due to the removal of moisture. The second weight loss of 16 wt % was taken place between 150–300°C due to the removal of adsorbed dopant anions. The third weight loss of 65 wt % was occurred between 300–500°C and attributed to the total decomposition of PRh chains, which is in accordance with the literature.[25] Needle like-TiO_2/PRh nanocomposite also showed weight losses at three stages. The first weight loss of 3 wt % was observed up to 50°C due to the removal of moisture. The second weight loss of 2 wt % was occurred between 380 and 450°C and attributed to the decomposition of organic

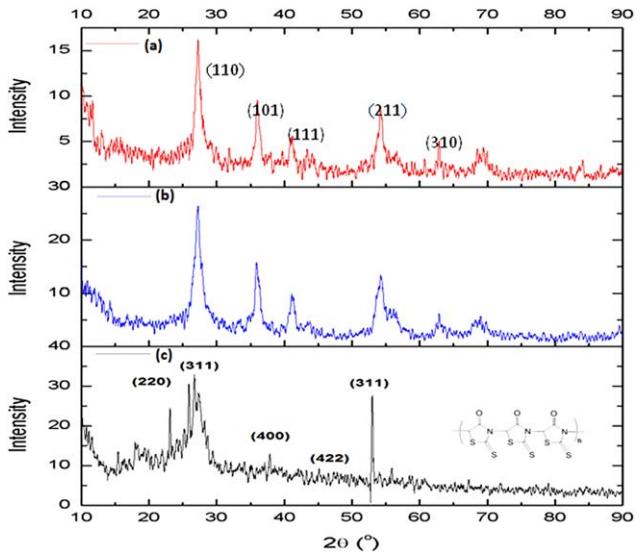

Figure 5. XRD patterns of (a) needle like-TiO_2, (b) needle like-TiO_2/PRh, and (c) PRh. [Color figure can be viewed in the online issue, which is available at wileyonlinelibrary.com.]

species present on the TiO_2 particles' surfaces. The third weight loss was observed between 600 and 700°C due to the total decomposition of nanocomposite structure. TGA analysis revealed that the thermal stability of TiO_2/PRh core/shell hybrid nanostructure was improved as a result of PRh interactions with TiO_2 nanoparticles surfaces. Similar thermal enhancement was reported by Kong et al., in a study carried out on γ-Fe_2O_3/PRh nanoparticles.[33] Also, the homogeneous dispersion of PRh chains on the surfaces of TiO_2 particles restricted the segmental motion of polymer chains and resulted in the enhanced decomposition temperature of TiO_2/PRh core/shell nanocomposite structure as desired.

XRD Analyses. The XRD patterns of needle like-TiO_2, needle like-TiO_2/PRh nanocomposite and PRh are depicted in Figure 5. The basic crystalline diffraction peaks of TiO_2 were observed at 27.4°, 36.1°, 41.2°, and 54.3° which correspond to (110), (101) (111), (211), and (002) planes of the rutile phase. These are in accordance with the data reported in the literature by Soundarrajan for growth of rutile TiO_2 nanorods on TiO_2 seed layer prepared by using facile low cost chemical methods.[34] The well-defined and sharp peaks in the XRD patterns of the rutile layer of TiO_2 confirmed its purity and degree of crystallinity. The XRD pattern of PRh shows crystalline diffraction peaks at 25.4° and 52.6° besides typical amorphous polymer peaks which are in accordance with the literature.[33] The XRD analysis of needle like-TiO_2/PRh does not provide discrimination between the patterns of needle like-TiO_2 and PRh clearly. It was noticed that the presence of PRh shells, proofed to be 2% by elemental analysis and TGA, has just intensified the XRD peaks of virgin needle like-TiO_2 particles on the nanocomposite structure [Figure 5(b)].[35] On the other hand, the presence of PRh shells on needle like-TiO_2 surfaces was previously demonstrated by XPS analyses (Figure 3). It was concluded that the characteristic

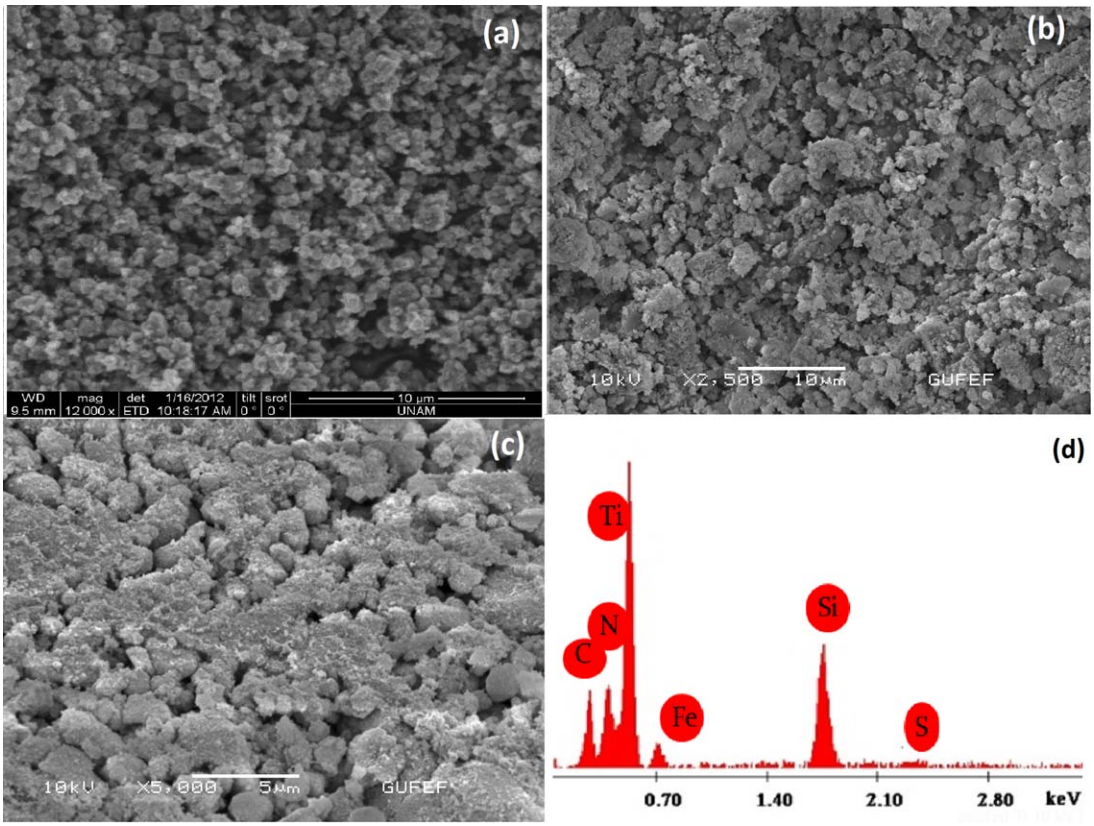

Figure 6. SEM micrographs of (a) needle like-TiO_2, (b) PRh, and (c) needle like-TiO_2/PRh, and (d) EDX images of needle like-TiO_2/PRh. [Color figure can be viewed in the online issue, which is available at wileyonlinelibrary.com.]

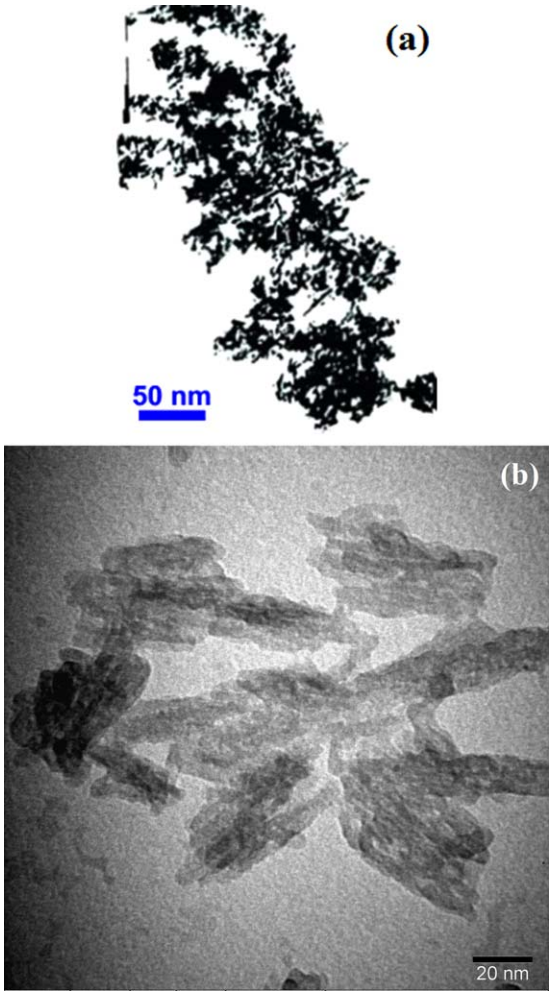

Figure 7. TEM micrographs of (a) needle like-TiO_2 and (b) needle like-TiO_2/PRh. [Color figure can be viewed in the online issue, which is available at wileyonlinelibrary.com.]

diffraction peaks of pristine TiO_2 were maintained after covering with thin PRh shells, indicating that TiO_2 morphology was unchanged after nanocomposite formation.

Electron Microscopy Analyses. SEM images of TiO_2 particles [Figure 6(a)], provided by Nanostructured and Amorphous Materials Inc. USA) revealed the needle like morphology of TiO_2 particles, aggregated morphology of PRh [Figure 6(b)] and homogeneously covered surfaces of needle like-TiO_2 particles by PRh shells as targeted [Figure 6(c)], which is also supported by TEM images, and in accordance with the SEM image of TiO_2 reported by Naldoni et al.[36] The elemental confirmation of needle like-TiO_2/PRh core/shell nanocomposite was evaluated using SEM-EDX mapping [Figure 6(d)]. The SEM-EDX mapping confirmed that Ti and Si peaks were due to the presence of TiO_2, Fe peak was due to the presence of $FeCl_3$ initiator molecules, N and C peaks were due to the presence of PRh chains on the needle like-TiO_2/PRh nanocomposite structure. Jooyoung et al., also reported similar EDX mapping for PRh in a study carried out with PRh modified anodic aluminum oxide membrane.[37]

TEM image of TiO_2 particles showed needle like and agglomerated morphology [Figure 7(a)], provided by Nanostructured and Amorphous Materials). TEM image of needle like-TiO_2/PRh nanocomposite [Figure 7(b)] revealed that surfaces of needle like-TiO_2 particles were covered with thin layer of PRh shells homogeneously, with a shell thickness ranging between 4.8 and 6.5 nm, and composed a core/shell structure which held by electrostatic interactions. Similar morphology was reported by Jooyoung et al., for silica/PRh core/shell nanocomposites.[5]

Contact Angle Measurement Results

The hydrophilic/hydrophobic characteristics of TiO_2, PRh, and needle like-TiO_2/PRh were determined by water contact angle measurements using pelleted discs (0.6 mm × 13 mm) and results obtained are given in Figure 8(a–c). Contact angle results of TiO_2, PRh, and needle like-TiO_2/PRh were determined to be 6.2°, 10°, and 13°, respectively which indicates the hydrophilic characters of the surfaces of all the samples. The contact angle value of needle like-TiO_2/PRh became bigger than both TiO_2 and PRh exhibiting the enhanced hydrophobicity of its surface which may be attributed to the enhanced surface roughness of TiO_2 particles, which is in accordance with the study reported by Niu for synthesis of sputtering TiO_2 films on poly (dimethylsiloxane) for surface modification.[38]

It is well known that contact angle values depend on the compositions of samples, sizes of the particles, numbers of pores on the surfaces of particles, capillary forces acting between the particles, the type of liquid, surface roughness of particles and the amount of —OH groups on the TiO_2 particles' surfaces, as reported by Yu on a study carried out on preparation and characterization of super-hydrophilic porous TiO_2 coating films.[39]

Conductivity Results

Conductivity values of the samples were determined by the four-probe technique using eq. (3).

$$\sigma = \frac{\ln 2}{\Pi d}\frac{I}{V} \tag{3}$$

The four-probe conductivities of TiO_2, PRh and needle like-TiO_2/PRh were calculated to be 2.5×10^{-6}, 7.2×10^{-2}, and 1.8×10^{-5} S cm^{-1}, respectively. The increase of conductivity of needle like-TiO_2/PRh may be attributed to the thin PRh shells on the surfaces of needle like-TiO_2 particles, which was determined to be 1.42% from elemental analysis measurements.

Electrokinetic Measurements Results

Effect of pH on ζ-Potentials. The effect of pH on ζ-potentials of needle like-TiO_2 and needle like-TiO_2/PRh nanocomposite (Figure 9) revealed that their ζ-potential values fell into the negative region.

At lower pH values, the ζ-potential of needle like-TiO_2 and needle like-TiO_2/PRh were shifted towards more positive values

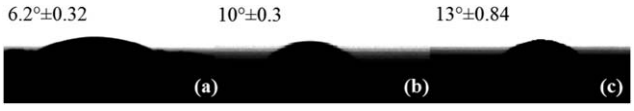

Figure 8. Contact angle measurements of (a) needle like-TiO_2, (b) PRh, and (c) needle like-TiO_2/PRh.

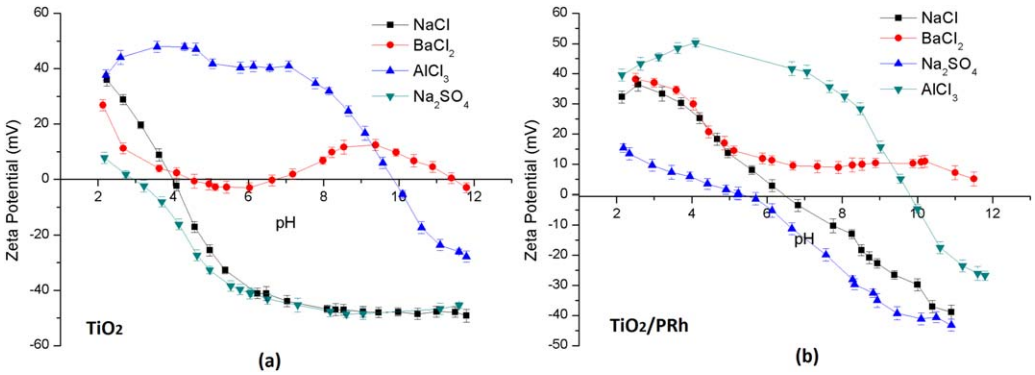

Figure 9. The effect of pH on ζ-potentials of (a) needle like-TiO_2 and (b) needle like-TiO_2/PRh colloidal dispersions with the presence of various salts ($T = 25°C$, $c_{salt} = 1 \times 10^{-3}$ *M*). [Color figure can be viewed in the online issue, which is available at wileyonlinelibrary.com.]

because of the adsorption of H_3O^+ ions onto the negatively charged surfaces of the dispersed particles. With the addition of $NaOH_{(aq)}$ solution into the dispersion media, OH^- anions increased the number of negative charges present and, as a result, the ζ-potential values shifted to more negative regions. Isoelectric points (IEP) of needle like-TiO_2 and needle like-TiO_2/PRh nanocomposite were determined to be 4.0 and 6.4, respectively which indicates that surfaces of needle like-TiO_2 particles were covered by PRh chains and formed core/shell structures.

Effect of Electrolytes on ζ-Potentials. Colloidal stability and particles' surface charge are important parameters for colloidal systems and this kind of information may be obtain via ζ-potential measurements. Effects of various anionic and cationic electrolytes (NaCl, Na_2SO_4, $BaCl_2$, $AlCl_3$) on ζ-potentials of needle like-TiO_2 and needle like-TiO_2/PRh nanocomposite particles were investigated and results obtained are depicted in Figure 10. Monovalent NaCl was observed to decrease the ζ-potentials of the samples by shifting to more positive regions but keeping the surface charge the same. Raised $NaCl_{(aq)}$ solution concentration compresses the electrical double layer of the dispersions and reduces the ζ-potentials. The same thing exists for Na_2SO_4 electrolyte. Divalent SO_4^{2-} anions shifted the ζ-potentials of the dispersions to more negative regions by causing a change on the surface charge of needle like-TiO_2/PRh nanocomposite particles. Increase in the concentration of divalent $BaCl_2$ reduced the ζ-potentials of the samples by shifting from negative regions to positive regions and also changing the surface charge after certain $BaCl_2$ concentrations. Tri-valent $AlCl_3$ changed the negative surface charge of needle like-TiO_2 particles to positive and already positive surface charge of needle like-TiO_2/PRh particles to more positive.

The effect of cationic and anionic electrolytes on ζ-potentials of needle like TiO_2 revealed that monovalent (Na^+) and divalent (Ba^{2+}) cations and monovalent (Cl^-) and divalent (SO_4^{2-}) anions were indifferent ions which only compressed the electrical double layer. On the other hand Al^{3+} ions may exist in non-hydroxyl forms below pH 4, and begin to hydrolyze. As pH increases above 4, hydroxyl complexes are formed (i.e., $Al(OH)^{2+}$, $Al(OH)^+_2$, $Al(OH)_3$, $Al(OH)_4$) which is also in accordance with the data reported in by Guzel et al., for polyindene/organo-montmorillonite conducting nanocomposites.[14]

Effect of Surfactants on ζ-Potentials. Effects of anionic SDS, cationic CTAB and non-ionic Triton X-100 surfactants on the colloidal properties of needle like-TiO_2 and needle like-TiO_2/PRh nanocomposite particles were investigated and results obtained are discussed below (Figure 11).

When CTAB was added into the needle like-TiO_2 dispersion, negatively charged surfaces of particles shifted to more positive regions starting from −31.8 mV and ending up with 7.63 mV at 20 ppm CTAB concentration. On the other hand, when CTAB solutions were added into needle like-TiO_2/PRh nanocomposite

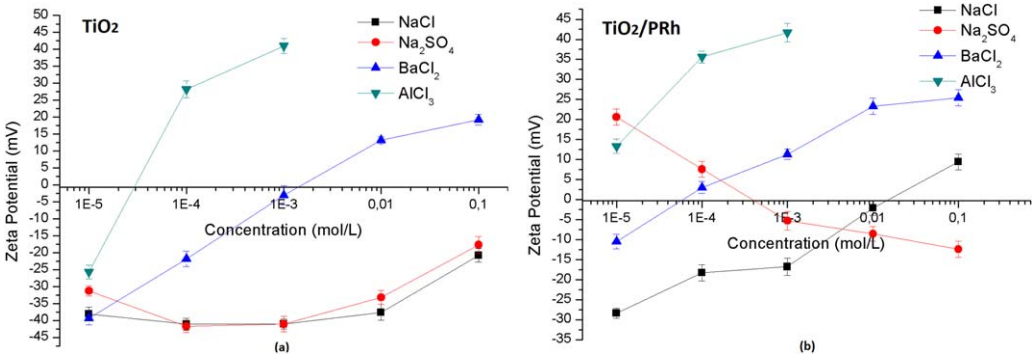

Figure 10. The effect of salt concentrations on ζ-potentials of (a) needle like-TiO_2 and (b) needle like-TiO_2/PRh colloidal dispersions. ($T = 25°C$, pH = 6). [Color figure can be viewed in the online issue, which is available at wileyonlinelibrary.com.]

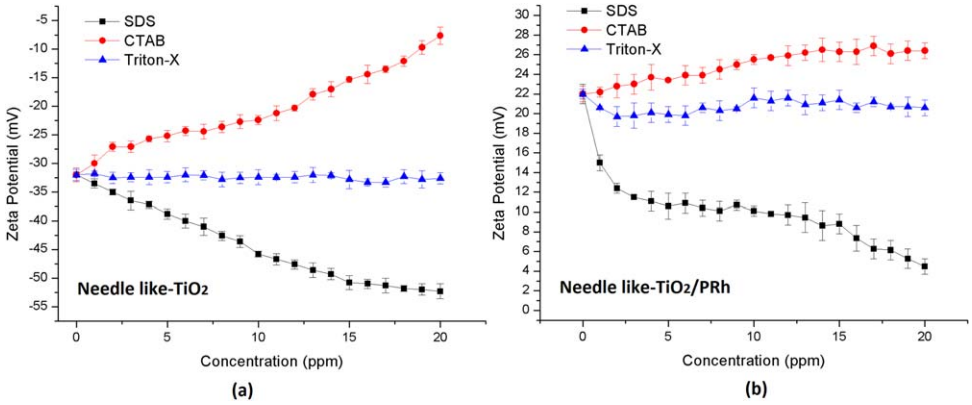

Figure 11. The effect of surfactant concentrations on ζ-potentials of (a) needle like-TiO_2 and (b) needle like-TiO_2/PRh colloidal dispersions. ($T = 25°C$, $c_{NaCl} = 1 \times 10^{-3}$ *M*). [Color figure can be viewed in the online issue, which is available at wileyonlinelibrary.com.]

dispersions, their ζ-potentials were started from 24 mV and ended up with 28.4 mV at 20 ppm CTAB concentration.

When SDS was added into the needle like-TiO_2 dispersion, its ζ-potential was started from −31.8 mV and ended up with −20.8 mV at 20 ppm SDS concentration. On the other hand, when SDS solution was added into needle like-TiO_2/PRh dispersion, the anionic head of the SDS surfactant interacted with the surfaces of the dispersed particles and started to shift the ζ-potential of nanocomposite particles from 24 mV to 4.47 mV with increasing SDS concentrations.

During the addition of non-ionic surfactant, Triton X-100 into the dispersion medium, ζ-potential values of needle like-TiO_2 and needle like-TiO_2/PRh were virtually unchanged, as expected.

Effect of Temperature on ζ-Potentials. Temperature has an effect on several parameters, including viscosity, ion adsorption, electrophoretic mobility of dispersed particles and their colloidal stability. At temperatures between 20°C and 50°C, however, the ζ-potentials of needle like-TiO_2 and needle like-TiO_2/PRh dispersions showed almost no change (Figure 12). The ζ-potentials were measured as −43.6 mV at 20°C and −35.6 mV at 50°C for needle like-TiO_2 and 11.1 mV at 20°C and 12.3 mV at 50°C for needle like-TiO_2/PRh nanocomposite dispersions, respectively. Positive ζ-potential values of needle like-TiO_2/PRh dispersions proof the covered surfaces of TiO_2 particles by PRh chains.

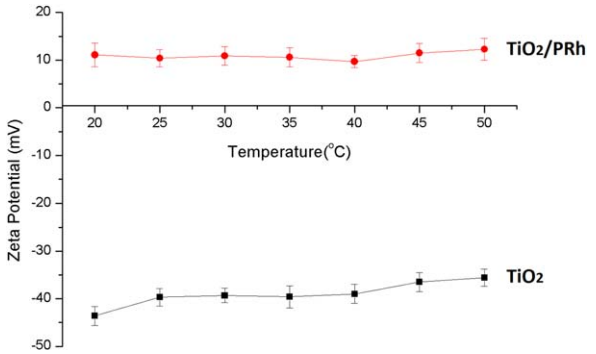

Figure 12. The effect of temperature on ζ-potentials of needle like-TiO_2 and needle like-TiO_2/PRh colloidal dispersions. ($c_{NaCl} = 1 \times 10^{-3}$ *M*). [Color figure can be viewed in the online issue, which is available at wileyonlinelibrary.com.]

Interactions of Nanoparticles with Bacteria and Antibacterial Results

TEM Results. It is well known that the cell membrane of bacteria composed of protein and enzymes which contain imidazole, amino, carboxyl, and thiol groups. These functional groups may electrostatically attract and anchor to the surface of needle like-TiO_2/PRh particles and cause the death of bacteria examined in this study. TEM experiments were one of the original approaches to demonstrate the above mentioned interactions between *E. coli* and needle like-TiO_2 and needle like-TiO_2/PRh nanoparticles. High magnification TEM image gave straight forward evidence to the immobilization of needle like-TiO_2 [Figure 13(a)] and needle like-TiO_2/PRh [Figure 13(b)] nanoparticles on the surfaces of *E. coli*. As is evident from the insets of TEM images as well, cell walls of all the *E. coli* cells were covered with lots of nanoparticles. In order to determine whether these nanoparticles have antibacterial effect or not, three different methods were applied and results obtained are discussed below.

Well Diffusion Method Results. No antimicrobial activities were determined for needle like-TiO_2, rhodanine and needle like-TiO_2/PRh nanoparticles samples against *E. coli, K. pneumoniae* and *S. aureus* with well diffusion method. This may be attributed to the low concentrations and inhomogeneous dispersion of nanoparticles in water in a Petri dish, which prevents the diffusion of dispersed nanoparticles into agar and do not inhibit the growth of bacteria.

Colony-Counting Method Results. The antibacterial activity tests were positive with colony-counting method for needle like-TiO_2 and rhodanine nanoparticles against the same bacteria and the data obtained are summarized in Table II. All the test compounds showed different antibacterial activities in vitro against the tested bacterial strains. Growth inhibition rates of needle like-TiO_2 and rhodanine were observed to enhance with increasing dispersed nanoparticles concentrations by tenfold for all the bacteria examined. The killing efficiency of *E. coli* was determined to be 95% for 0.1 g mL^{-1} needle like-TiO_2/PRh

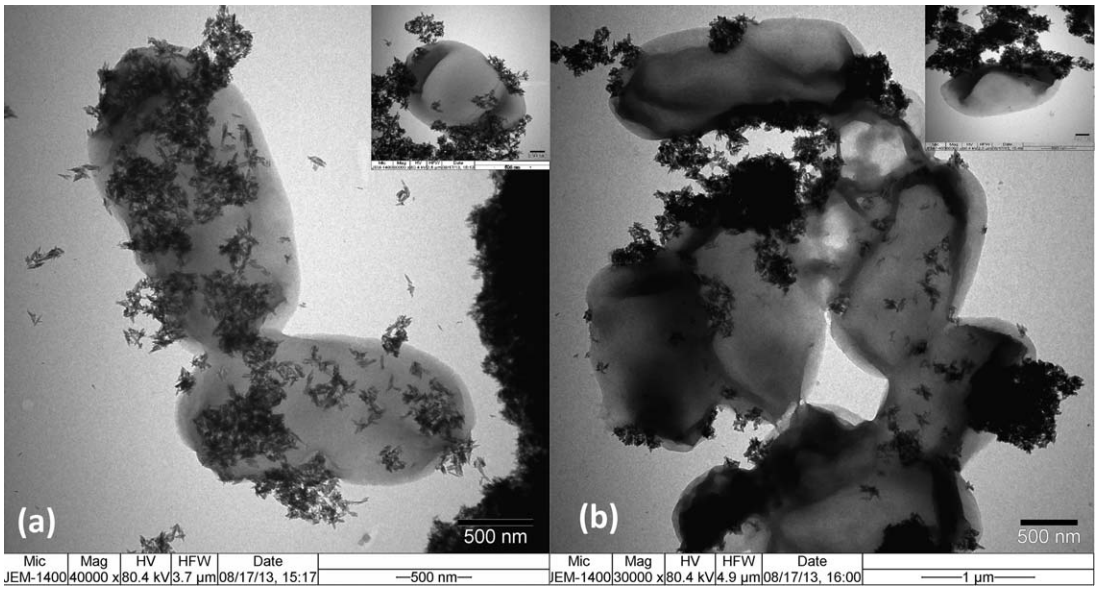

Figure 13. TEM image of *E. coli* immobilized on (a) needle like-TiO_2 and (b) needle like-TiO_2/PRh nanoparticles.

nanocomposite, which is an excellent antibacterial activity when compared with needle like-TiO_2 and rhodanine nanoparticles.

Disc Diffusion Method Results. The antimicrobial activities of needle like-TiO_2 and rhodanine against the same bacteria were also tested by measuring the zone of inhibition in modified Kirby-Bauer disc diffusion method and results obtained are given in Table III. No antibacterial activity was determined for needle like-TiO_2 nanoparticles after 24 h of incubation against *S. aureus*. It is well known that all the types of TiO_2 nanoparticles show antimicrobial activities due to their photo catalytic activities if determined under UV light. The experiments of present study were carried out under day light conditions and according to our observations on antimicrobial activities of other geometries of TiO_2 nanoparticles, antibacterial activity depends also on the geometry and size of the materials but it needs further investigations.

Table II. Growth Inhibition Rates of Needle Like-TiO_2, Rhodanine and Needle Like-TiO_2/PRh Against *K. pneumoniae, E. coli* and *S. aureus*

	Killing efficiencies of bacterial strains (24 h)		
Compounds [Concentrations, mg/mL]	*E. coli* (G–)	*K. pneumoniae* (G–)	*S. aureus* (G+)
Needle like-TiO_2/PRh [0.1]	0.95	0.67	0.49
Rhodanine [0.01]	0.43	0.32	0.50
Rhodanine [0.1]	0.45	0.55	0.53
Needle like-TiO_2 [0.01]	0.30	0.55	0.54
Needle like-TiO_2 [0.1]	0.48	0.54	0.62

Rhodanine and needle like-TiO_2/PRh nanocomposite particles were led to a clearly visible zone of inhibition against *S. aureus* (Figure 14) with average zone diameters of 18 mm and 12 mm, respectively. These results indicate that, after coating with PRh shells of average thicknesses of 4.8–6.5 nm, needle like-TiO_2 nanoparticles have become successfully antibacterial active against *S. aureus*. This may be attributed to the tertiary amide groups of PRh shells. It is known that these amide groups can be partially protonated in aqueous media and develop positive charges on PRh chains, which interact with negatively charged bacteria cell walls and lead to the death of the bacteria examined. The differences in zone diameters also suggest that rhodanine had better antimicrobial activity against *S. aureus* than needle like-TiO_2/PRh nanocomposites. Same kind of antibacterial activity was not observed for *K. pneumoniae* which may be attributed to the capsule layer of the bacterium.[40] Similar inhibitory effects against *S. aureus* and *E. coli* were reported for TiO_2 nanoparticles by Ye et al.[41]

It was noticed that the solubilities of the dispersed particles in water were low and formed suspensions but not perfect solutions. This partial solubility caused the observation of divergent antibacterial activity results against the three bacteria examined by three different methods. For example disc diffusion method showed good antibacterial activity against *S. aureus* in which

Table III. Antibacterial Activity of Rhodanine and Needle Like-TiO_2/PRh Against *E. coli, K. pneumoniae, S. aureus* With Disc Difusion Method

	Diameter of zone (mm)		
Sample	*E. coli*	*K. pneumoniae*	*S. aureus*
Needle like-TiO_2/PRh	10	-	12
Rhodanine	14	14	18
Needle like-TiO_2	-	-	-

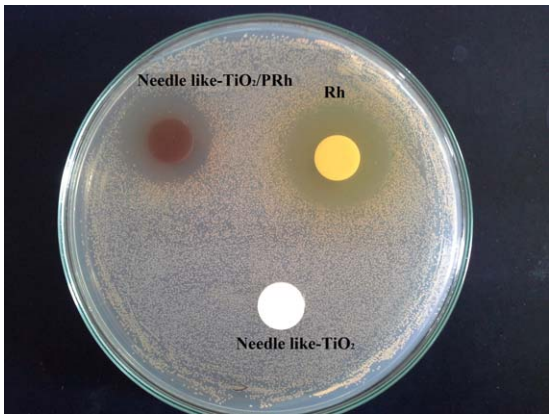

Figure 14. Photograph of bacterial colonies formed by *S. aureus* treated with the needle like-TiO_2/PRh nanoparticles, rhodanine, and needle like-TiO_2. [Color figure can be viewed in the online issue, which is available at wileyonlinelibrary.com.]

needle like-TiO_2/PRh nanoparticles were used as solid pellets in disc shaped. Needle like-TiO_2/PRh nanoparticle dispersions were also showed good antibacterial activity against *E. coli* with colony-counting method. One of the reasons for these divergent antibacterial activity results may be attributed to the needle-like morphology of TiO_2. It was reported in the literature by Masuda et al., that the morphologies of TiO_2 nanoparticles affect its surface area, surface crystal faces (i.e., Miller indices), molecular absorptivity properties and electron mobilities.[42]

CONCLUSIONS

Needle like-TiO_2/PRh core/shell nanocomposites held by electrostatic interactions were successfully synthesized and characterized with various techniques. Their electrokinetic properties revealed the formations of colloidally stable aqueous dispersions and solved the well-known agglomeration problem of these kinds of systems. Positive and enhanced antibacterial activity for needle like-TiO_2/PRh core/shell conducting nanoparticles were determined against three bacteria by colony-counting method which indicates that this nanocomposite could be a good candidate material for future long-term antibacterial applications and may be supported with further in vivo tests. The future work on TiO_2/PRh core/shell nanocomposite will be the preparation of its colloidal dispersions in silicone oil and evaluations of electrokinetic, dielectric, electrorheological, vibration damping and creep-recovery properties.

ACKNOWLEDGMENTS

The authors are grateful to the Turkish Scientific and Technological Research Council (111 T 637) and COST Action CM1101 for the support of this study.

REFERENCES

1. Dallas, P.; Sharma, V. K.; Zboril, R. *Adv. Colloid Interface.* **2011**, *166*, 119.
2. Kong, H.; Jang, J. *Biomacromolecules* **2008**, *9*, 2677.
3. Song, J.; Kong, H.; Jang, J. *J. Colloid Interf. Sci.* **2011**, *359*, 505.
4. Song, M.-X.; Zheng, C.-J.; Deng, X.-Q.; Wang, Q.; Hou, S.-P.; Liu, T.-T.; Xing, X.-L.; Piao, H.-R. *Eur. J. Med. Chem.* **2012**, *54*, 403.
5. Song, J.; Song, H.; Kong, H.; Hong, J.-Y.; Jang, J. *J. Mater. Chem.* **2011**, *21*, 19317.
6. Song, M. X.; Zheng, C. J.; Deng, X. Q.; Sun, L-P.; Wu, Y.; Hong, L.; Li, Y-J.; Liu, Y.; Wei, Z. Y.; Jin, M. J.; Piao, H. R. *Eur. J. Med. Chem.* **2013**, *60*, 376.
7. Maness, P.-C.; Smolinski, S.; Blake, D. M.; Huang, Z.; Wolfrum, E. J.; Jacoby, W. A. *Appl. Environ. Microbiol.* **1999**, *65*, 4094.
8. Grigorieva, A. V.; Goodilin, E. A.; Dubova, K. L.; Anufrieva, T. A.; Derlyukova, L. E.; Vyacheslavov, A. S.; Tretyakov, Y. D. *Solid State Sci.* **2010**, *12*, 1024.
9. Kiyono, H.; Tsumura, T.; Kiyo, T.; Toyoda, M.; Shimada, S. *Ceram. Int.* **2011**, *37*, 1813.
10. Wei, W.; Chunhua, L.; Mingxing, S.; Yaru, N.; Zhongzi, X. *Chin J. Catal.* **2012**, *33*, 629.
11. Gordon, T. R.; Cargnello, M.; Paik, T.; Mangolini, F.; Weber, R. T.; Fornasiero, P.; Murray, C. B. *J. Am. Chem. Soc.* **2012**, *134*, 6751.
12. Sun, A.; Li, Z.; Li, M.; Xu, G.; Li, Y.; Cui, P. *Powder Technol.* **2010**, *201*, 130.
13. Yu, H. K.; Eun, T. H.; Yi, G.-R.; Yang, S.-M. *J. Colloid Interf. Sci.* **2007**, *316*, 175.
14. Guzel, S.; Unal, H. I.; Erol, O.; Sari, B. *J. Appl. Polym. Sci.* **2012**, *123*, 2911.
15. Guo, M.; Zheng, C.-J.; Song, M.-X.; Wu, Y.; Sun, L.-P.; Li, Y.-J.; Piao, H.-R. *Bioorg. Med. Chem. Lett.* **2013**, *23*, 4358.
16. Bhat, J. A.; Tenguria, R. K. *World J. Pharm. Res.* **2014**, *3*, 230.
17. Ko, W.-C.; Paterson, D. L.; Sagnimeni, A. J.; Hansen, D. S.; Gottberg, A. V.; Mohapatra, S.; Casellas, J. M.; Goossens, H.; Mulazimoglu, L.; Trenholme, G.; Klugman, K. P.; McCormack, J. G.; Yu, V. L. *Emerg. Infect. Dis.* **2002**, *8*, 160.
18. Mühldolfer, I.; Blum, G.; Donohue-Rolfe, A.; Heier, H.; Olschlager, T.; Tschape, H.; Wallner, U.; Hacker, J. *Res. Microbiol.* **1996**, *147*, 625.
19. Tenover, F. C. *Am. J. Med.* **2006**, *119*, 3.
20. Moritz, M.; Geszke-Moritz, M. *Chem. Eng. J.* **2013**, *228*, 596.
21. Chapman, J. S. *Int. Biodeter. Biodegr.* **2003**, *51*, 133.
22. Munoz-Bonilla, A.; Fernández-García, M. *Prog. Polym Sci.* **2012**, *37*, 281.
23. Tamer, U.; Cetin, D.; Suludere, Z.; Boyacı, I. H.; Temiz, H. T.; Yegenoglu, H.; Daniel, P.; Dinçer, I.; Elerman, Y. *Int. J. Mol. Sci.* **2013**, *14*, 6223.
24. Su, W. S.; Wei, S.; Hu, S. Q.; Tang, J. X. *J. Hazard. Mater.* **2009**, *172*, 716.
25. Kardas, G.; Solmaz, R. *Appl. Surf. Sci.* **2007**, *253*, 3402.
26. Sun, A.; Li, Z.; Li, M.; Xu, G.; Li, Y.; Cui, P. *Powder Technol.* **2010**, *201*, 130.
27. Patrocinio, A. O. T.; Paniago, E. B.; Paniago, R. M.; Iha, N. Y. M. *Appl. Surf. Sci.* **2008**, *254*, 1874.

28. Kruse, N.; Chenakin, S. *Appl. Catal. A-Gen.* **2011**, *391*, 367.
29. Martin, H. J.; Schulz, K. H.; Bumgardner, J. D.; Walters, K. B. *Appl. Surf. Sci.* **2008**, *254*, 4599.
30. Cruz-Silva, R.; Amaro, E.; Escamilla, A.; Nicho, M. E.; Sepulveda-Guzman, S.; Arizmendi, L.; Romero-Garcia, J.; Castillon-Barraza, F. F.; Farias, M. H. *J. Colloid. Interf. Sci.* **2008**, *328*, 263.
31. Song, Y.-Y.; Hildebrand, H.; Schmuki, P. *Surf. Sci.* **2010**, *604*, 346.
32. Archana, D.; Singh, B. K.; Joydeep, D.; Dutta, P. K. *Carbohydr. Polym.* **2013**, *95*, 530.
33. Kong, H.; Song, J.; Jang, J. *Chem. Commun.* **2010**, *46*, 6735.
34. Soundarrajan, P.; Sankarasubramanian, K.; Logu, T.; Sethuraman, K.; Ramamurthi, K. *Mater. Lett.* **2014**, *116*, 191.
35. Bagheri, S.; Shameli, K.; Hamid, S. B. A. Composite Nanoparticles. In J. Chem.; Calandra, P., Parola, V. L., Liveri, V. T., Lidorikis, E., Finocchi, F., Eds.; Hindawi Publishing Corporation, **2013**; Vol. *2013*, Chapter 6, pp 1.
36. Naldoni, A.; Minguzzi, A.; Vertova, A.; Santo, V. D.; Borgese, L.; Bianchi, C. L. *J. Mater. Chem.* **2011**, *21*, 400.
37. Song, J.; Oh, H.; Kong, H.; Jang, J. *J. Hazard. Mater.* **2011**, *187*, 311.
38. Niu, Z.; Gao, F.; Jia, X.; Zhang, W.; Chen, W.; Qian, K. Y. *Colloid Surf. A* **2006**, *272*, 170.
39. Yu, J.; Zhao, X.; Zhao, Q.; Wang, G. *Mater. Chem. Phys.* **2001**, *68*, 253.
40. Amako, K.; Meno, Y.; Takade, A. *J. Bacteriol.* **1988**, *170*, 4960.
41. Ye, Q.; Gao, T.; Wan, F.; Yu, B.; Pei, X.; Zhou, F.; Xue, Q. *J. Mater. Chem.* **2012**, *22*, 13123.
42. Masuda, Y.; Ohji, T.; Kato, K. *Cryst. Growth Des.* **2010**, *10*, 913.